KSME

Springer

Journal of Mechanical Science and Technology 34 (2) 2020

Original Article
DOI 10.1007/s12206-020-0115-6

Keywords:
· Additive manufacturing
· TIG welding
· Wire feeding orientation
· Thin-wall
· Dimensional accuracy
· Mechanical properties

Correspondence to:
Nitish P. Gokhale
p2016416@pilani.bits-pilani.ac.in

Citation:
Gokhale, N. P., Kala, P., Sharma, V., Palla, M. (2020). Effect of deposition orientations on dimensional and mechanical properties of the thin-walled structure fabricated by tubgsten inert gas (TIG) welding based additive manufacturing process. Journal of Mechanical Science and Technology 34 (2) (2020) 701~709. http://doi.org/10.1007/s12206-020-0115-6

Received July 26th, 2019
Revised November 1st, 2019
Accepted December 1st, 2019

† Recommended by Editor Chongdu Cho

Effect of deposition orientations on dimensional and mechanical properties of the thin-walled structure fabricated by tungsten inert gas (TIG) welding-based additive manufacturing process

Nitish P. Gokhale[1], Prateek Kala[1], Varun Sharma[2] and Murali Palla[1]

[1]Department of Mechanical Engineering, Birla Institute of Technology and Science, Rajasthan, India, [2]Department of Mechanical and Industrial Engineering, Indian Institute of Technology, Roorkee, Uttarakhand, India

Abstract Welding-based additive manufacturing can potentially produce a cost-effective process for the production of dense metallic parts. Tungsten inert gas (TIG) welding-based additive manufacturing process uses wire as a filler material and offers a high deposition rate with low spattering. In this study, different orientations of wire feeding nozzle and TIG welding torch, such as front wire feeding (FWF), back wire feeding (BWF), and side wire feeding (SWF), were investigated for thin-walled metal deposition with enhanced dimensional accuracy and mechanical properties. The dimensional accuracy of thin-walls deposited at four different orientations were investigated in terms of deposition height and deposition width. The FWF orientation with higher wire feeding angle and SWF orientation produced poor dimensional accuracy in the deposition. FWF orientation with normal wire feeding angle and BWF orientation provided a decent dimensional accuracy and surface appearance. The deposited samples exhibited a similar trend for Vickers microhardness, residual stress, and microstructure for the four different wire feeding orientations.

1. Introduction

Additive manufacturing techniques have been widely investigated by researchers to fabricate metallic parts at low cost and less time. Additive manufacturing directly produces the metallic components with mechanical properties comparable with parts produced by conventional casting process [1]. The metal additive manufacturing process involves the use of powder or wire as raw material. Most of the industrial processes, including selective laser sintering, direct metal laser sintering (DMLS) [2], and laser engineered net shaping (LENS) [3] uses powder as a raw material. These processes use a laser source for melting powder particles to obtain the required shape. The mechanical characterization of the powder-based additive manufacturing process has been done by several researchers. Ferreri et al. [4] studied the effect of build orientation on the mechanical properties for powder bed fusion-based metal deposition process. Fotovvati et al. [5] studied the correlation between shape, size, and geometrical accuracy of the structure deposited using the powder-based process. With decreasing size of the structure, the error in the dimensional accuracy also decreases. The use of wire as a filler material and arc welding source, such as gas metal arc welding or gas tungsten arc welding, has emerged as an alternative to laser-based processes. Wire-based processes have advantages in operational cost, near-net geometrical shape, and higher density of parts over other additive manufacturing processes. The wastage of raw material has also been eliminated by implementing wire arc-based additive manufacturing processes [6]. The welding sources have higher energy efficiency than any other commercial energy sources, such as laser or electron beam. However,

Table 1. Chemical composition of the filler wire material.

Material	Chemical compositions (wt. %)						
	Si	Mn	P	S	C	Fe	Cu
Q235 (substrate)	≤ 0.3	0.30-0.70	≤ 0.045	≤ 0.045	0.420-0.50	Remaining	-
ER70S-6 (deposited material)	0.80-1.15	1.4-1.85	0.025	0.035	0.06-0.15	Remaining	0.05

the synchronization of feeder wire and welding torch is a difficult task to control for arc-based processes. The metal deposition at micro-level is a complicated process in wire arc additive manufacturing compared with powder-based processes due to the higher energy and larger size of the heat-affected zone. The control of the temperature while layer by layer deposition is also easier in powder-based processes. The deposition height is affected by temperature gradients generated in arc welding-based metal deposition process [7].

Among the arc welding processes, tungsten inert gas (TIG) welding process has an arc efficiency of 68 %. The MIG-based additive manufacturing process has higher material deposition rate than TIG-based additive manufacturing process but suffers from spattering defects. The force exerted by the arc is among the crucial issues in the case of MIG-based additive manufacturing process [8]. The deposition width yields from MIG welding-based additive manufacturing process has been reported higher than TIG-based metal deposition. In TIG welding-based metal deposition system, filler wire and TIG torch need to be controlled separately. Lu et al. [9] characterized welding-based additive manufacturing process in terms of microstructure study, tensile testing, and hardness testing. However, few authors [10, 11] investigated the residual stress induced in the parts produced by arc welding-based additive manufacturing. Most authors observed tensile residual stress along the surface [12]. Same et al. [13] reviewed the metallurgy of the metal additive manufacturing. They mentioned that compressive residual stress has been observed in the core part of the deposited structure when measured through its thickness. Hagqvist et al. [14] studied the effect of positioning of the tip position of the feeding wire on the quality of deposition. The effect of the different positions of wire feeding on the deposition process has been studied.

Researchers have not considered the effect of different deposition orientations on geometrical and mechanical properties of the deposited structures. In the present work, the TIG welding-based additive manufacturing process is selected for experimentation. The effect of orientation of TIG welding torch and wire feeding nozzle on the surface appearance and mechanical properties of the deposited structure was investigated. The effect of four different orientation of wire feeding nozzle with TIG torch was investigated for geometrical and mechanical properties. The dimensional accuracy, surface appearance, and mechanical characterization, such as microhardness test, microstructure analysis, and residual stress responsible for the fatigue life of the deposited material, were examined in the following sections.

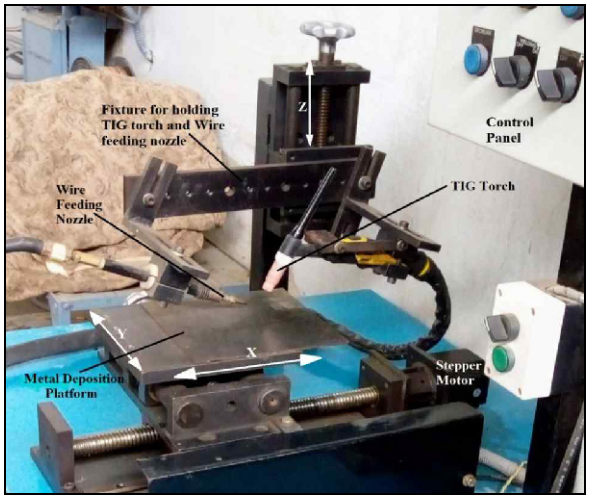

Fig. 1. Experimental setup fabricated in-house for TIG-based additive manufacturing process.

2. Materials and methods

The experimental setup used in this study consisted of three main parts (Fig. 1). This setup consisted of metal deposition platform, holding fixture for welding torch, and wire feeding nozzle, control system. The metal deposition platform moved in X and Y-axis, respectively. The movement of the platform in X-axis was controlled using the stepper motor. The thin-walled structures were fabricated by movement of the metal deposition platform. The work holding fixture was moved up after deposition of one layer by a distance equal to the height of the deposited layer. The holding fixture has a provision to change the angle made by wire feeding nozzle and TIG torch with the substrate. The holding fixture for torch and wire feeding nozzle is attached to the Z-axis (Fig. 1). The control system was used for automatic control of the process when metal is being deposited. The coordination between the metal deposition platform and holding fixture for controlled deposition were implemented using this control system. The ESAB Caddy 2200i welding machine was used for deposition. The electrode, to work piece distance, was kept constant at 2.5 mm for this study. Argon gas with a flow rate of 10 L/min was supplied to act as a shielding gas for the molten metal pool.

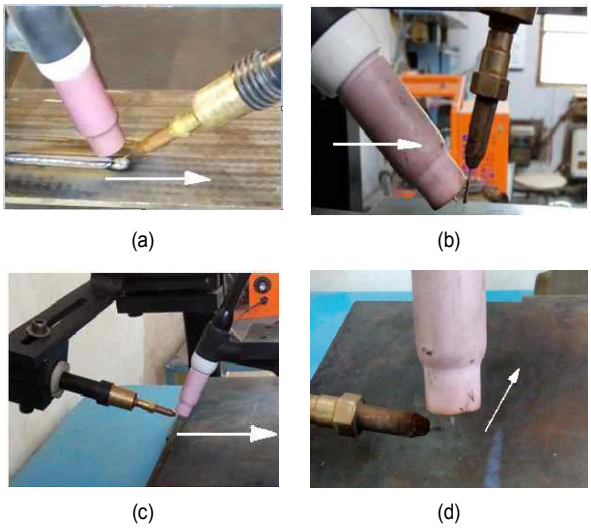

Fig. 2. (a) Orientation 1: FWFNA; (b) orientation 2: FWFHA; (c) orientation 3: BWF; (d) orientation 4: SWF.

The base plate of low carbon steel, with dimensions 150 mm × 150 mm and thickness of 6 mm, was used as a substrate material. The surface of the substrate was cleaned with acetone solution to avoid rusty surfaces. The wire of material ER70S-6 with 1.2 mm diameter was used as a filler material. The chemical composition of the substrate and filler materials are shown in Table 1.

Three main orientations were identified in the present study, as follows: front wire feeding (FWF); back wire feeding (BWF); and side wire feeding (SWF) method. The FWF orientation was further divided into two types as front wire feeding with normal wire feeding angle (FWFNA), and front wire feeding with higher wire feeding angle (FWFHA). Orientations 1 and 2, namely, FWFNA and FWFHA, used the same wire feeding method, which is the front feeding method. BWF was used as orientation 3, and SWF was used as orientation 4.

The angle made by the wire feeding nozzle with the substrate in FWFNA was 18°, whereas in FWFHA, the angle made by the wire feeding nozzle was set to 85°. In this case, the wire feeding angle was changed to analyze the effect of another orientation at the same wire feeding method. The selected four orientations are shown in Fig. 2. In FWFNA (Fig. 2(a)) and FWFHA (Fig. 2(b)), wire feeding was done from the front side of the TIG torch. The wire feeding was done from the backside of the TIG torch in BWF (Fig. 2(c)), whereas in SWF (Fig. 2(d)), wire feeding was done from the left side of the deposition path.

The width of the deposition was measured using Celestron digital microscope PRO with CMOS sensor-based mechanism for capturing clear images. The maximum resolution of this system is 5 megapixels. The microscope was calibrated before using it for measurements and was set to the magnification of 20x while capturing images. The height of the deposition was measured using the digital height gauge with a resolution of 0.01 mm. Samples for the microhardness and residual stress tests were obtained from the material deposited at four different orientations. The samples were cut using wire EDM (electron discharge machining) to avoid generating excessive residual stresses due to cutting forces. The cut samples were placed in moulds, and electropolishing was done on the top surface of the sample to obtain an enchased parallel surface. The testing of residual stress was conducted using X-ray diffraction method at National Texture facility in IIT Bombay, India. The same samples were tested for microhardness at Atlanta Metallurgical services, Kolhapur, India. The microhardness of all four samples manufactured at four orientations were investigated. Microhardness testing was conducted using vickers microhardness tester. The load of 300 gf was applied for 10 s for this test, because the material utilized was low carbon steel. The testing machine used was automated and showed error in measurements up to 4 %. The microstructure was analyzed for all four samples at the same facility under a metallurgical microscope.

Table 2. Optimum values of process parameters set for metal deposition.

Sr. No.	Process parameters	Value
1	Current	70 A
2	Torch movement velocity	3.5 cm/min.
3	Wire feeding speed	1 m/min
4	Voltage	16 V
5	Arc gap (electrode to substrate distance)	2.5 mm
6	Flow rate of shielding gas	10 L/min.
7	Shielding gas	Argon (100 %)
8	Substrate plate thickness	6 mm
9	Tungsten electrode diameter (2 % thorium)	2.4 mm
10	Layer increment after deposition of each layer	2.5 mm
11	Angle made by the TIG torch with the substrate	75°

Based on the pilot experimentation, suitable values of process parameters were identified and kept the same for deposition using all four orientations, as shown in Table 2. The output characteristics of samples deposited using four different orientations were studied. A study of dimensional accuracy, microhardness, residual stress induced in the thickness of the deposited samples, and microstructures of the deposited structure was also performed.

3. Results and discussions

Results of the investigation on dimensional accuracy and mechanical properties, including microhardness, microstructure analysis, and residual stress induced in the thickness of samples deposited at four different orientations, were discussed in this section. The manufactured, multilayered thin-walled samples were measured for dimensional accuracy. The front and top views of the thin-walled samples deposited at four different orientations are shown in Fig. 3.

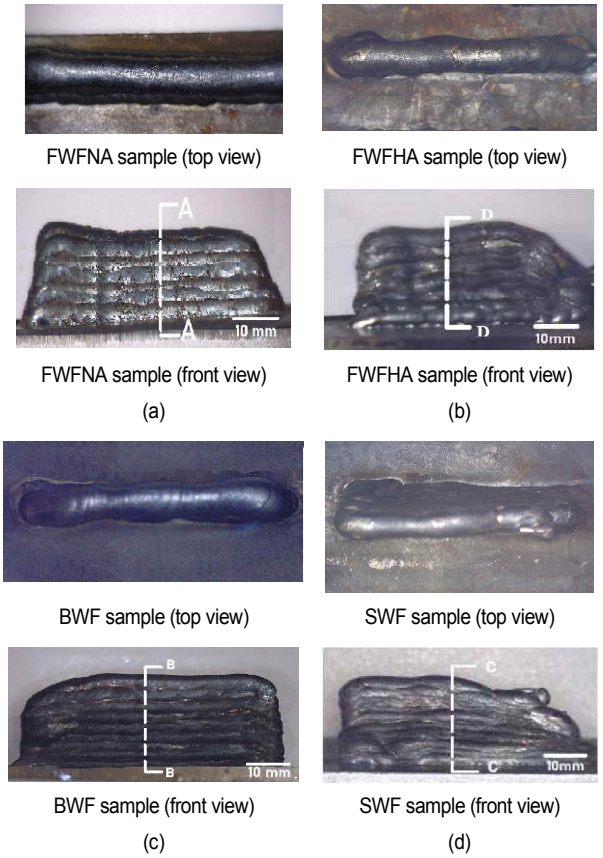

Fig. 3. Front view of the deposited thin-walled structures: (a) Orientation 1: FWFNA; (b) orientation 2: FWFHA; (c) orientation 3: BWF; (d) orientation 4: SWF.

3.1 Geometrical accuracy and surface appearance

The surface appearance of the deposited thin-walled structure was inspected visually for front view, and cross-section view. The surface appearance of the thin walls deposited using FWFNA and BWF were better than samples deposited using SWF and FWFHA. Samples deposited at orientation FWFNA and BWF were free from defects, such as spattering, thereby showing that all of the layers have been deposited with ease. The cross-section views of all samples are shown in Fig. 4. The cross-section of the specimens deposited at orientation FWFNA and BWF were better than other two orientations (Figs. 4(a) and (c)). However, an irregular profile was observed in the cross-section of the sample deposited using FWFHA. This observation was due to the possibility that the force exerted by filler material at higher feeding angle dislocates the molten material even during the on-going deposition. As shown in Fig. 4(d) and top view in Fig. 3(d), the thin-walled sample deposited at SWF, which utilized a side wire feeding method made an angle with the substrate plate. For SWF orientation, when the deposition process was in progress, molten droplets tended to flow away from the path of deposition and in the wire feeding direction due to the inertia of filler wire. The path of the deposition for the next layer was offset from the path of the deposition of the previous layer. Therefore, the overall height of the deposited wall was lower compared with other orientations indicated in Table 3.

Table 3. Dimensional parameter measurements of the deposited walls at four different orientations.

Orientation	Width (mm)	Height (mm)
FWFNA	4.15 ± 0.15	15.85 ± 0.35
FWFHA	4.50 ± 0.35	15.6 ± 0.40
BWF	3.55 ± 0.10	18.20 ± 0.30
SWF	4.45 ± 0.30	9.85 ± 0.60

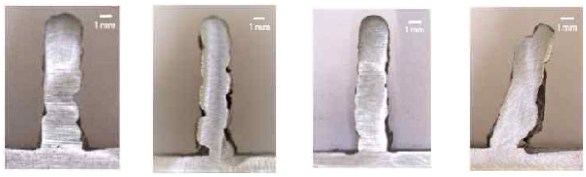

Fig. 4. Cross section of the samples for (a) orientation 1: FWFNA (AA); (b) orientation 2: FWFHA (DD); (c) orientation 3: BWF (BB); (d) orientation 4: SWF (CC).

At the end of the deposition, a gradual decrease in the deposition height due to excessive heat was observed among all orientations, which was highly significant in case of orientation FWFNA, FWFHA, and SWF. However, this was controlled by developing a feedback control strategy for deposition [15]. The dimensional accuracy for the samples manufactured at four different orientations was investigated. The measurements of deposition width and deposition height were taken at a distance of 10 mm on top of the surface. The Celestron digital microscope was utilized for these measurements at a magnification of 20x after calibration. The elaborated results of the measurements are shown in Table 3. The measurements observed showed that BWF had less dimensional variation. The thin-walled multilayered deposition with a length up to 50 mm was produced using BWF orientation and possessed the thinnest deposition width of 3.55 ± 0.10 mm and the highest deposition height of 18.20 ± 0.30 mm. The TIG-based process produced the thinnest wall, which was free from spattering defects.

The variation in deposition height and deposition width was shown in Figs. 5 and 6. The graphs showed that the variation in deposition height and deposition width of the sample deposited at FWFNA and BWF were less significant.

The deposition can also be done using FWFNA and combination of FWFNA and BWF, as shown in Figs. 7(a) and (b), respectively. As shown in Fig. 7(b), the combination of FWFNA and BWF can be used for continuous deposition of parts with varying geometrical features. This technique may be helpful when FWFNA and BWF are used in combination, because this provides the freedom to move in forward and backward directions, thereby helping with the performance of continuous metal deposition in less time.

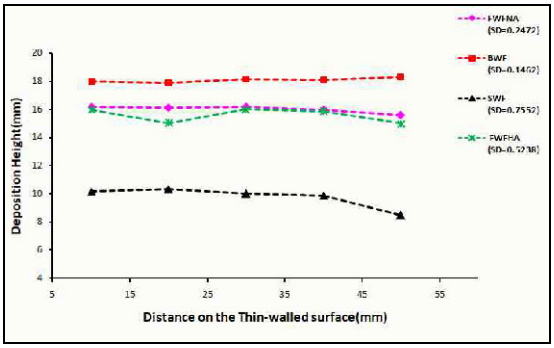

Fig. 5. Variation in the height of the deposited thin-walled structure.

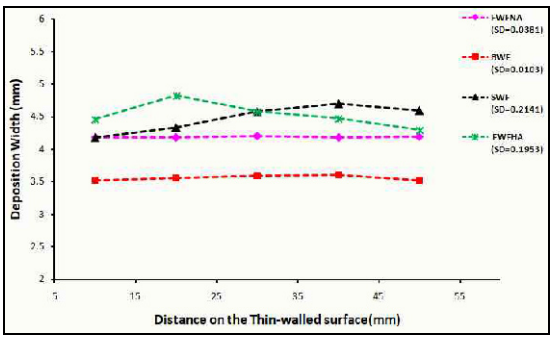

Fig. 6. Variation in the width of the deposited thin-walled structure.

(a) (b)

Fig. 7. (a) Deposition scheme using FWFNA; (b) deposition scheme using a combination of FWFNA and orientation 2.

3.2 Microhardness test

The samples prepared for the characterization were investigated for microhardness using ASTM standard (ASTM-E-384-17). The points chosen for the measurement are shown in Fig. 8. Fig. 9 shows the variation in microhardness along the height of deposition for the samples deposited at four different orientations. The highest value of microhardness was observed in the sample deposited at FWFNA (i.e., up to 250 HV). The overall increasing trend was observed in the microhardness results. When one layer is deposit over another layer, the part of the previously deposited layer is partially re-melted during deposition of the next layer, but the cooling rate of the top layer is higher than the previously deposited layer. Thus, the smooth granular structure was formed in the top layer, which led to an increase in hardness. The same case happened for each successive layer in the deposition.

3.3 Residual stress measurement

To understand the fatigue life of deposited samples, residual

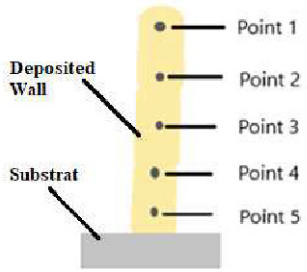

Fig. 8. Points chosen for measurement of residual stress and microhardness.

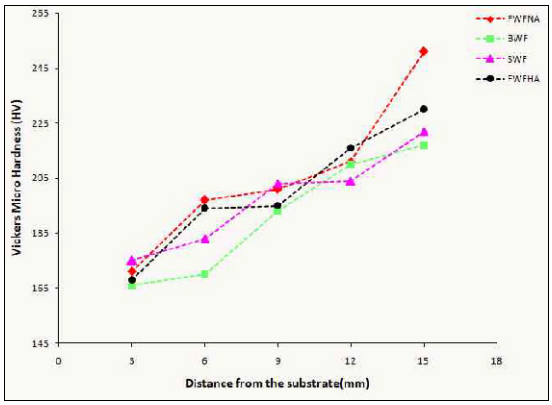

Fig. 9. Distribution of vickers microhardness in all four samples.

stress testing was performed. The residual stresses are the stresses retained in the sample manufactured by welding-based additive manufacturing processes due to irregular thermal cycling. The distribution of the residual stresses may change from the base plate to the top surface of the build structure. In general, residual stress observed in parts fabricated using additive manufacturing process depends on the energy density applied during deposition [16] and the type of method used for deposition. In this work, TIG welding-based additive manufacturing process was used for the metal deposition. The residual stress measurements were conducted using X-ray diffraction machine. The sample was taken from the build wall cross-section. The points equidistant to each other were marked for the measurement of the residual stress (Fig. 8). The residual stress was calculated using $\sin^2\psi$ method. In this method, $\sin^2\psi$ value was plotted against lattice spacing value. Fig. 10 shows the plot of lattice spacing against the $\sin^2\psi$ value for point 1 in FWFHA orientation sample. The slope of the straight line drawn on the plot provides the value of residual stress and expressed in the form of stress tensor, as shown in Eq. (1).

$$\begin{bmatrix} \sigma_{xx} & T_{xy} & T_{xz} \\ T_{yx} & \sigma_{yy} & T_{yz} \\ T_{zx} & T_{zy} & \sigma_{zz} \end{bmatrix} = \begin{bmatrix} -235.0 & 0 & 32.1 \\ 0 & -121.8 & 140.6 \\ 32.1 & 140.6 & 0 \end{bmatrix} \quad (1)$$

where σ_{xx} denotes transverse stress, σ_{yy} is longitudinal stress,

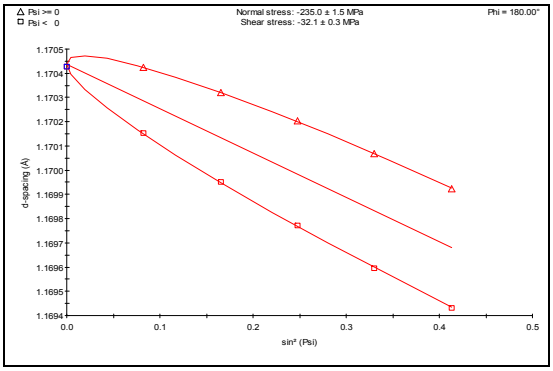

Fig. 10. Plot of $\sin^2\psi$ Vs d-spacing (for residual stress measurements).

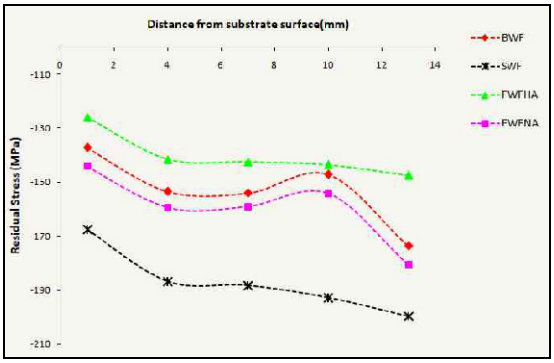

Fig. 11. Residual stress induced in samples produced at four orientations.

and σ_{zz} represents normal stress. The average residual stress, which is also called hydrostatic residual stress, is calculated using the following equation:

$$\sigma_{\text{hydrostatic stress}} = (\sigma_{xx} + \sigma_{yy} + \sigma_{zz})/3 \quad (2)$$

Therefore, the value of hydrostatic residual stress (i.e., $\sigma_{\text{hydrostatic stress}}$) at point 1 of the FWFHA sample was calculated (using Eq. (2)) as 120 Mpa. The same method was used for all other points in all orientations samples.

Fig. 11 shows the distribution of residual stress in the sample manufactured at four different orientations. For all four orientations, compressive residual stress was observed. The value of compressive residual stress increases, as we move from the substrate surface to the top part. The compressive residual stresses observed in the sample were good for the fatigue life of the parts. The metal deposition in this study was performed at a lower current range. Therefore, less heat was accumulated in the material during deposition. Solid-state phase transformation, which occurs because of the low heat input, may lead to compressive residual stresses in the core part of deposited structure [17]. This change in residual stress was explained with the correlation between microhardness and residual stress testing results. Bottommost layers are subjected to higher number of heating and cooling cycles, thereby resulting in lower residual stress. This phenomenon is common to most of the 3D printing technologies, either using metal or plastic as a raw material. The observed variation in the residual stress from substrate surface to top surface further supported the correlation exists between microhardness and residual stress, which was also observed by other researchers. Comparing Figs. 9 and 11, the residual stress value was more compressive at higher values of hardness in the deposited material. According to literature, compressive residual stress decreased gradually with increasing hardness of the material [18]. Moreover, the hardness value increased simultaneously with decreasing residual stress. Thus, more compressive residual stress and higher hardness value in the component is beneficial to obtain a higher fatigue life. Also, the residual stress in FWFNA orientation was more compressive than other samples. This observation can be explained using Fig. 12. When the metal deposition was conducted using FWFNA orientation, the deposition direction and the direction of the feeding wire were opposite each other, as shown in Fig. 12(a). The region "A" represents deposited material, "B" represented the molten material, and "C" represented the material coming out of the wire feeding nozzle to be melted. Hence, due to the motion of the feeding wire in the opposite direction, the material in region C exerts force on the region B (i.e., molten material). Considering this compressive force, more compressive residual stress was induced in FWFNA sample than any other orientation sample. Alternatively, in BWF orientation (Fig. 12(b)), wire feeding direction and deposition direction are the same. Thus, region B is not subjected to as much compressive force as in FWFNA.

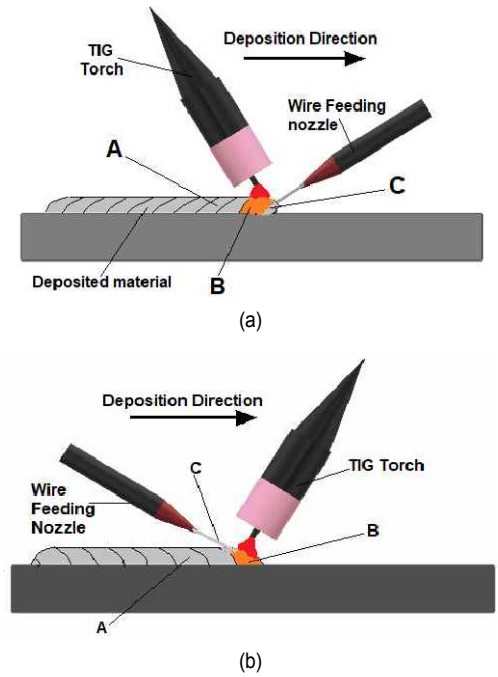

Fig. 12. Physical condition at the time of deposition using (a) orientation FWFNA; (b) orientation BWF.

Table 4. Results of microstructure analysis.

Sr. No.	Type of grains determined in the observation	ASTM grain size number	Volume fraction (by %)		
			Ferrite (%)	Pearlite (%)	Other (%)
Sample 1: (FWFNA)	Equiaxed-Ferritio-Pearlitic grains	9-9.5	83.80	16.20	NIL
Sample 2: (FWFHA)	Equiaxed-Ferrito-Pearlitic grains	9-9.5	79.75	20.25	NIL
Sample 3: (BWF)	Equiaxed-Ferrito-Pearlitic grains	9-9.5	77.50	22.50	NIL
Sample 4: (SWF)	Equiaxed-Ferrito-Pearlitic grains	9-9.5	74.90	25.10	NIL

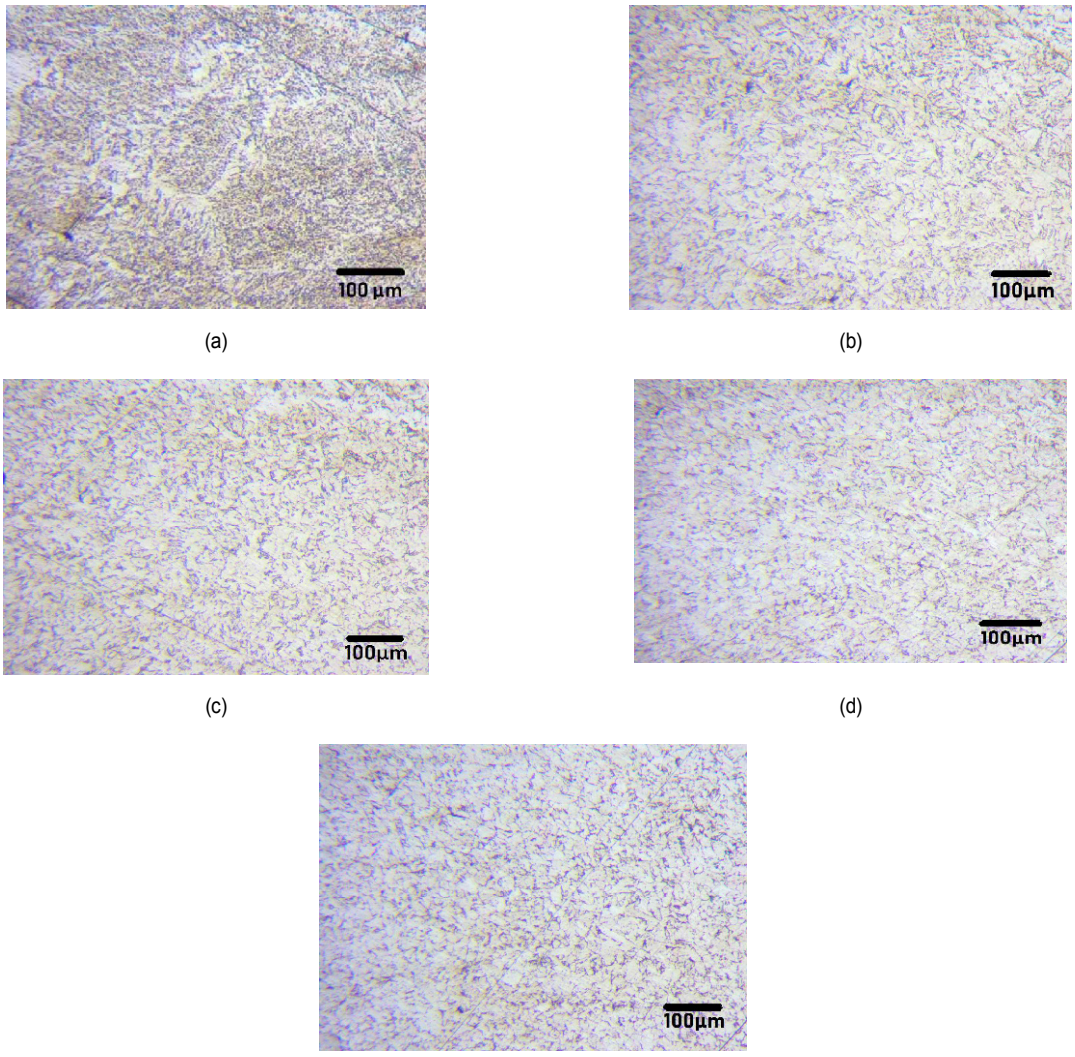

(a) (b) (c) (d) (e)

Fig. 13. Microstructure observed at (a) point 1; (b) point 2; (c) point 3; (d) point 4; (e) point 5.

3.4 Microstructure analysis

The microstructure analysis for all four samples was done at the points indicated in Fig. 8. Five points equidistant to each other were selected for this analysis. The microstructure analysis was conducted to obtain the volume fraction in the deposited material (ASTM-E-124503). The grain size measurements (ASTM-E-112-13) were obtained for all four samples. The volume fractions and grain size number of all four samples are presented in Table 4. The actual percentage of carbon was

calculated from this data; 0.13 % carbon was present in the deposited structure, which lies within the limit specified in the material properties of ER70S-6 (i.e., 0.06 %-0.15 %).

A similar microstructure was observed for samples deposited at all four orientations. The ASTM grain size numbers of 9 to 9.5 was observed in samples deposited at all four orientations, thereby indicating fine grain size.

The Widmanstatten structure was observed (Fig. 13(a)) at point 1 in the top layer of samples deposited at all four orientations, because the top layer in the deposition undergoes a single heating cycle, which further leads to faster cooling of the deposited material due to the flow of argon gas in the TIG arc-based deposition process. However, the layers beneath the top layer are subjected to simultaneous heating and cooling cycles.

The equiaxed-ferrito-pearlite structure was observed at point 2 to point 4, as indicated in Fig. 8 in the layers beneath the top layer (Figs. 13(b)-(e)). The ferrite and pearlite were mainly observed in the samples at those points. This process can be used to generate 3D parts with uniform mechanical properties throughout the deposition, except for the top layer, which was easily removed by any post-processing method.

4. Conclusion

Four orientations of wire feeding nozzle and TIG torch were examined to fabricate thin-walled structures. Two forms of front wire feeding method were compared for deposition. The thin-walled metallic structures were deposited for all four orientations and investigated for deposition quality in terms of dimensional accuracy, microhardness, residual stress, and microstructure. Based on the results, the following conclusions were drawn:

(1) FWFNA (18°) orientation was better than FWFHA (85°) in terms of dimensional accuracy and surface form properties.

(2) The combination of orientation FWFNA with BWF will produce free-form geometrical parts with improved geometrical accuracy and surface appearance with minimum fabrication time.

(3) The Vickers microhardness test showed a similar trend for all four orientations. The highest hardness value was observed in the part deposited at FWFNA and BWF.

(4) The compressive residual stress was reported in the deposited structures when measured through its thickness due to the irregular intervals of heating and cooling cycles.

(5) The fine equiaxed-ferrito-pearlite grains were observed in the microstructure. Ferrite and pearlite were observed at 74 %-84 % and 16 %-25 %, respectively, which significantly fulfilled the material property requirements for ER706S. The Widmanstatten ferrite structure was observed on the top portion of the deposited wall due to faster cooling of molten metal in the last layer.

Acknowledgements

The authors are gratefully acknowledging the Central Workshop facility and financial support from Research Initiation Grant of Birla Institute of Technology and Science, Pilani, India-333031.

Nomenclature

TIG	: Tungsten inert gas welding
FWFNA	: Front wire feeding with normal wire feeding angle
FWFHA	: Front wire feeding with higher wire feeding angle
BWF	: Back wire feeding
SWF	: Side wire feeding
σ_{xx}	: Transverse stress
σ_{yy}	: Longitudinal stress
σ_{zz}	: Normal stress
$\sigma_{hydrostatic\ stress}$	: Hydrostatic residual stress

References

[1] D. Ding, Z. Pan, S. V. Duin, H. Li and C. Shen, Fabricating superior NiAl bronze components through wire arc additive manufacturing, *Materials,* 9 (8) (2016) 652.

[2] A. Simchi, F. Petzoldt and H. Pohl, On the development of direct metal laser sintering for rapid tooling, *J. Mater. Process. Technol.,* 141 (3) (2003) 319-328.

[3] W. Liu and J. N. DuPont, Fabrication of functionally graded TiC/Ti composites by laser engineered net shaping, *Scr. Mater.,* 48 (9) (2003) 1337-1342.

[4] N. C. Ferreri, S. Ghorbanpour, S. Bhowmik, R. Lussier, J. Bicknell, B. M. Patterson and M. Knezevic, Effects of build orientation and heat treatment on the evolution of microstructure and mechanical properties of alloy Mar-M-509 fabricated via laser powder bed fusion, *Int. J. Plast.,* 121 (2019) 116-133.

[5] B. Fotovvati and E. Asadi, Size effects on geometrical accuracy for additive manufacturing of Ti-6Al-4V ELI parts, *Int. J. Adv. Manuf. Technol.,* 104 (5-8) (2019) 2951-2959.

[6] D. Ding, Z. Pan, D. Cuiuri and H. Li, Wire-feed additive manufacturing of metal components: Technologies, developments and future interests, *Int. J. Adv. Manuf. Technol.,* 81 (1-4) (2015) 465-481.

[7] J. Xiong and G. Zhang, Adaptive control of deposited height in GMAW-based layer additive manufacturing, *J. Mater. Process. Technol.,* 214 (4) (2014) 962-968.

[8] Y. Li, J. Xiong and Z. Yin, Molten pool stability of thin-wall parts in robotic GMA-based additive manufacturing with various position depositions, *Robot. Comput. Integr. Manuf.,* 56 (2019) 1-11.

[9] X. Lu, Y. F. Zhou, X. L. Xing, L. Y. Shao, Q. X. Yang and S. Y. Gao, Open-source wire and arc additive manufacturing system: Formability, microstructures, and mechanical properties, *Int. J. Adv. Manuf. Technol.,* 93 (5-8) (2017) 2145-2154.

[10] F. Martina, M. J. Roy, B. A. Szost, S. Terzi, P. A. Colegrove, S. W. Williams, P. J. Withers, J. Meyer and M. Hofmann, Residual stress of as-deposited and rolled wire+arc additive manufacturing Ti-6Al-4V components, *Mater. Sci. Technol.*

(United Kingdom), 32 (14) (2016) 1439-1448.
[11] J. R. Hönnige, P. A. Colegrove, S. Ganguly, E. Eimer, S. Kabra and S. Williams, Control of residual stress and distortion in aluminium wire + arc additive manufacture with rolling, *Addit. Manuf.,* 22 (2018) 775-783.
[12] Z. Wang, E. Denlinger, P. Michaleris, A. D. Stoica, D. Ma and A. M. Beese, Residual stress mapping in Inconel 625 fabricated through additive manufacturing: Method for neutron diffraction measurements to validate thermomechanical model predictions, *Mater. Des.,* 113 (2017) 169-177.
[13] W. J. Sames, F. A. List, S. Pannala, R. R. Dehoff and S. S. Babu, The metallurgy and processing science of metal additive manufacturing, *Int. Mater. Rev.,* 61 (5) (2016) 315-360.
[14] P. Hagqvist, A. K. Christiansson and A. Heralić, Automation of a laser welding system for additive manufacturing, *IEEE Int. Conf. Autom. Sci. Eng.* (2015) 900-905.
[15] Y. M. Zhang, P. Li, Y. Chen and A. T. Male, Automated system for welding-based rapid prototyping, *Mechatronics,* 12 (1) (2002) 37-53.
[16] L. M. Sochalski-Kolbus, E. A. Payzant, P. A. Cornwell, T. R. Watkins, S. S. Babu, R. R. Dehoff, M. Lorenz, O. Ovchinnikova and C. Duty, Comparison of residual stresses in inconel 718 simple parts made by electron beam melting and direct laser metal sintering, *Metall. Mater. Trans. A Phys. Metall. Mater. Sci.,* 46 (3) (2015) 1419-1432.
[17] S. Paddea, J. A. Francis, A. M. Paradowska, P. J. Bouchard and I. A. Shibli, Residual stress distributions in a P91 steel-pipe girth weld before and after post weld heat treatment, *Mater. Sci. Eng. A,* 534 (2012) 663-672.
[18] P. Fu, R. Chu, Z. Xu, G. Ding and C. Jiang, Relation of hardness with FWHM and residual stress of GCr15 steel after shot peening, *Appl. Surf. Sci.,* 431 (2018) 165-169.

Prateek Kala is an Assistant Professor at BITS Pilani, India in the Mechanical Engineering Department. He obtained his Ph.D. from IIT Delhi in the Mechanical Engineering Department. He completed M. Tech. in Production and Industrial Systems Engineering from Mechanical Engineering Department IIT Roorkee. He works in the area of advanced manufacturing process. He has performed experimental investigation in the area of ultrasonic drilling, magnetic abrasive finishing, and is currently working on 3D printing of metal parts using arc welding process. He has published research articles in various peer-reviewed journals in the field of advanced manufacturing and abrasive finishing.

Murali Palla worked on metallic glasses during his Ph.D. from IISc Bangalore and continued his work in IHPC Singapore as a research scientist. He has ten publications in some of the top Journals in this area. He has also published three papers on phase-field modeling of fracture in bio-composites. Currently, he has worked at BITS Pilani-Pilani Campus, Rajasthan since 2013 working as an Assistant Professor. He has expertise in atomistic modeling, mechanical testing experiments, and phase-field modelling and possesses a good understanding of the constitutive behavior of metallic glass.

Varun Sharma is an Assistant Professor at the Indian Institute of Technology, Roorkee, Mechanical Engineering Department. He obtained his Ph.D. in the field of ultrasonic-assisted turning from IIT Delhi. He works in the area of Additive Manufacturing for Mechanical and biomedical application and is currently working in 3D printing of biomedical implants. He has published peer-reviewed research papers and a book chapter in various international journals and conferences.

Nitish Gokhale obtained his B.E. in Mechanical Engineering and M.Tech. in Mechatronics from VIT University Vellore, India. He is pursuing his Ph.D. in the field of Additive Manufacturing at BITS-Pilani, India. His research areas are additive manufacturing and advanced manufacturing processes.